ISSN 1392–1207. MECHANIKA. 2022 Volume 28(2): 145–151

Experimental Research and Fatigue Life Prediction of Ultra-High-Strength Steel Aermet100

Enze ZHU*, Hu CHEN, Xingbo FANG***, Hong NIE******

*College of Aerospace Engineering, Nanjing University of Aeronautics and Astronautics, Nanjing 210016, China, E-mail: zhuenze@nuaa.edu.cn

**College of General Aviation and Flight, Nanjing University of Aeronautics and Astronautics, Liyang 213300, China, E-mail: chen_hu@nuaa.edu.cn (Corresponding author)

***College of Aerospace Engineering, Nanjing University of Aeronautics and Astronautics, Nanjing 210016, China, E-mail: fangxignbo@nuaa.edu.cn

****College of Aerospace Engineering, Nanjing University of Aeronautics and Astronautics, Nanjing 210016, China, State Key Laboratory of Mechanics and Control of Mechanical Structures, Nanjing 210016, China. E-mail: hnie@nuaa.edu.cn

crossref http://dx.doi.org/10.5755/j02.mech.29302

1. Introduction

One of the hot topics in solid mechanics is the simulation of fracture and damage phenomena. When the engineering structure is under high loading, the principal stress may exceed the material strength, which will lead to progressive failure. The failure processes of these materials are characterized by various failure mechanisms, such as the fracture process zone (FPZ) in rock and concrete, the shear band localization in ductile metals, or discrete crack discontinuities in brittle materials. In the past few decades, the accurate modelling and evolution of fuzzy discontinuities and discrete discontinuities have been a hot interest for researchers.

Xu [1, 2] et al. Tested the dynamic fracture toughness of 30CrMnSiNi2A high strength steel under impact load with different loading rates by an experimental and numerical method and studied the rate correlation. The experimental results show that 30CrMnSiNi2A Steel exhibits ductile fracture characteristics to a large extent. The dynamic fracture toughness increases clearly with the increase of loading rate. In this paper, the experimental phenomena are observed, but the influence of the loading rate on the dynamic fracture toughness is not studied in depth from the theoretical and numerical simulation. Sun [3] studied the ultra-low cycle impact fatigue life of Aermet100 steel notched specimens under impact load. Based on continuous damage mechanics, an improved life prediction model was proposed, and the modified elastic deformation energy and cumulative plastic strain rate were simplified to predict the fatigue life of metal samples under large impact load. However, the model used in his paper is not suitable for analyzing the influence of different load rates on crack growth and the number of life cycles. He [4] studied the effect of loading rate on low-cycle fatigue properties of turbine rotor steel, the results show that with the loading rate increases, the cyclic stress of the rotor steel increases, and low-cycle fatigue life increases too. However, the experiment data was merely fitted through the Coffin-Manson formula without considering the damage evolution and crack initiation, and the strain rate effect was also ignored.

To furtherly study the effect of loading rate on the fatigue properties of Aermet100 steel from the theoretical and numerical simulation, this paper established a dynamic constitutive model of Aermet100 steel to consider the load rate effect, the parameters of J-C equations are also obtained through some material tests. Unlike the previous work, this paper introduced XFEM combined with the J-C model defined a user-defined subroutine to predict the fatigue life of Aermet100 steel specimens under different loading rates. Lab fatigue tests are carried out, which verify the correctness of the simulation model. Based on the lab tests and simulation model, the relationship between the loading rate and the fatigue life is obtained, respectively.

2. Material, mechanical property test and dynamic constitutive model

The materials and methods section should contain sufficient detail so that all procedures can be repeated. It may be divided into headed subsections if several methods are described.

2.1. Material

Aermet100 steel (23Co4Ni2Cr3MoE) is a kind of iron-nickel alloy. It has ultra-high-strength, excellent plane strain fracture toughness, stress corrosion cracking resistance, and good weldability. It is the most competitive material for key bearing components of aircraft and is usually used to manufacture aircraft landing gear and turbine shafts.

However, Aermet100 steel is a strain rate sensitive material. For materials, the strain rate sensitivity has nothing to do with the structure, only with the basic properties of the material.

Marsh and Campbell [3] investigated the dynamic tensile behaviour of low-carbon mild steel specimens when a fracture is known. The upper and lower yield limits increase with increasing strain rate, as observed by Manjoine [4]. However, although the strength limit also increases, it increases slowly. Therefore, the strain strengthening of mild steel decreases with the increase of strain rate under large tensile strain and high strain rate. In fact, except for the upper yield stress, the behaviour of the material at high strain rates looks like an ideal plastic material with little or no strain hardening.

2.2. Tests

MTS static tensile testing machine was used to carry out static tensile tests on the Aermet100 steel sample, and the basic material properties and engineering stress-strain curves were obtained as shown in Fig. 1, including elastic modulus, yield strength, ultimate tensile strength, plastic elongation and section shrinkage. According to the ASTM-638 standard, the displacement-controlled loading was carried out under the displacement sensor. The average yield strength of Aermet100 steel is 1620MPa.

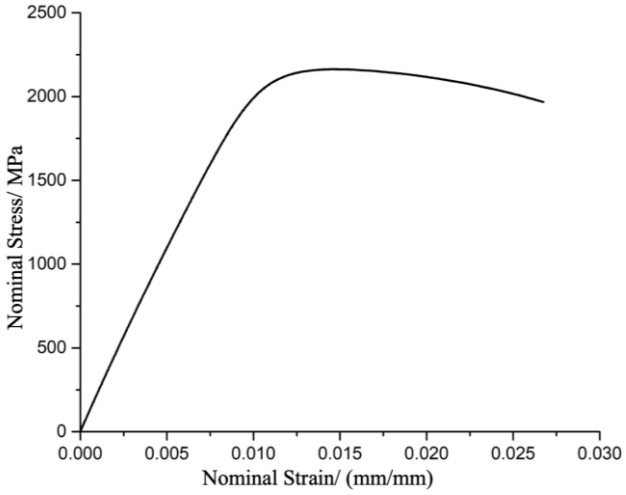

Fig. 1 Nominal stress vs. strain curve of Aermet100 under tensile load

Aermet100 steel has a typical elongation under uniaxial tension, and its necking occurs when the stress reaches the maximum. There exists an equivalence between the nominal stress-strain relationship and the true stress-strain relationship before necking. After necking, the deformation is in the necking area. The stress state changes from a unidirectional stress state to multiaxial when it is necking. Equivalence doesn't exist between the true stress-strain relationship and the nominal stress-strain relationship.

Through the basic principles of mechanics of materials, we can transform the nominal (engineering) stress-strain ($\sigma_e - \varepsilon_e$) relationship into the true stress-strain ($\sigma_{true} - \varepsilon_{true}$) relationship. The transformation method is shown in Formula 1, 2.

$$\begin{aligned} \sigma_e &= \frac{f}{A_0} \\ \varepsilon_e &= \frac{d}{l_0} \end{aligned}, \tag{1}$$

$$\begin{aligned} \sigma_{true} &= \frac{fl}{A_0 A_c} = \sigma_e(1+\varepsilon_e) \\ \varepsilon_{true} &= ln\left(\frac{l}{l_0}\right) = ln(1+\varepsilon_e) \end{aligned}, \tag{2}$$

Marsh and Campbell [3] investigated the dynamic tensile behaviour of low-carbon mild steel specimens when a fracture is known. The upper and lower yield limits increase with increasing strain rate, as observed by Manjoine [4]. However, although the strength limit also increases, it increases slowly. Therefore, the strain strengthening of mild steel decreases with the increase of strain rate under large tensile strain and high strain rate. In fact, except for the upper yield stress, the behaviour of the material at high strain rates looks like an ideal plastic material with little or no strain hardening.

Where: f is tensile load; A_0 is initial area (before necking); d is elongation length; l_0 is initial length; A_c is area (after necking); l is total length. Fig. 3 shows the true stress-strain relationship through transformation.

Through tensile tests and equivalent transformation, the average properties of Aermet100 steel under the quasi-static load test are listed in Table 1. These parameters are obtained from the experiment data fitting, and then we can calculate the confidence value (R squared), which is 0.85. It should be noted that the ultimate load was recorded during the test and the fracture strain was measured and treated after the test. E is elastic modulus; σ_b is tensile strength; $\sigma_{0.2}$ is yield strength; Rupt.ε_p is rupture strain.

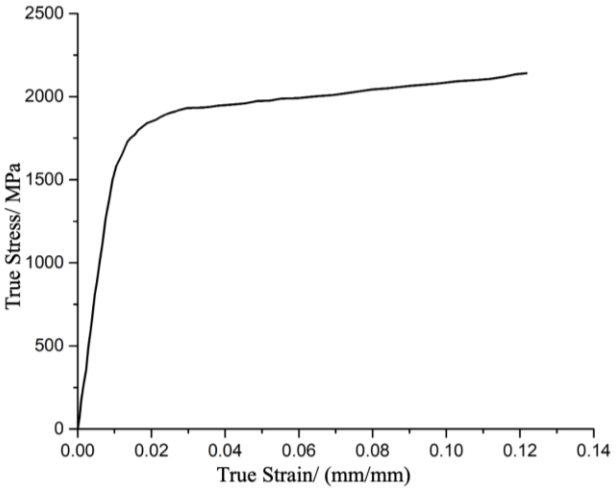

Fig. 2 True stress vs. strain curve of Aermet100 under tensile load

Table 1

Mechanical properties of Aermet100 steel

E, GPa	$\sigma_{0.2}$, MPa	σ_b, MPa	Rupt.ε_p
190.15	1620.59	1930.25	0.1088

2.3. Dynamic constitutive model

Before applying the dynamic constitutive model, the yield stress and plastic stress-strain relationship under different strain rates should be determined first. Johnson-Cook's phenomenological constitutive model [6] is usually used to describe the dynamic mechanical behaviour of materials. The form of the model equation is simple, and the parameters can be easily obtained through the simple mechanic's experiment of materials.

$$\sigma_y = (A + B\varepsilon_p^n)(1 + C ln\dot{\varepsilon}^*)(1 - T^{*m}), \tag{3}$$

where: A, B, C, n and m are the material constants determined from the curve measured by the test. A, B and n denote the flow hardening of the alloy material. C represents the strain rate effect and m describes the temperature sensitivity. In the above formula, σ_y is Von-Mises equivalent stress; ε_p^n is the equivalent plastic strain; $\dot{\varepsilon}^*$ and T^* are di-

mensionless plastic strain rate and temperature, respectively.

The basic equations of Johnson-Cook's constitutive equation in solving material deformation include the listed parts (Hooke's law of elasticity, the law of flow, the uniaxial fundamental equation, the uniaxial stress integration method), which are also necessary for the ABAQUS user-defined material subroutine.

2.4. Material tests and parameters determination

The parameters A, B and n can be obtained by fitting the compression test data of Aermet100 steel samples under quasi-static reference strain rate ($10^{-3}s^{-1}$ generally) and corresponding reference temperature (generally 298K). Under such experimental conditions, the Johnson-Cook constitutive model equation can be simplified as following:

$$\sigma = A + B\varepsilon^{n}. \tag{4}$$

Under this condition, when there is no plastic strain, the yield stress of Aermet100 steel is $A = \sigma = \sigma_s$ and σ_s is the true yield strength of the material under such conditions. The following formula can be deduced by taking natural logarithms on both sides of the equation by moving terms.

$$ln(\sigma - A) = ln(B) + nln\varepsilon. \tag{5}$$

From the above formula, the original $\sigma - \varepsilon$ curve can be transformed into $ln(\sigma - A) - ln(\varepsilon)$ curve, and the $ln(B)$ value can be obtained by the intercept between the straight line and the longitudinal axis, and the slope is the value n. As shown in Fig. 3, the R^2 (R-Squared) value of curve fitting is 0.9.

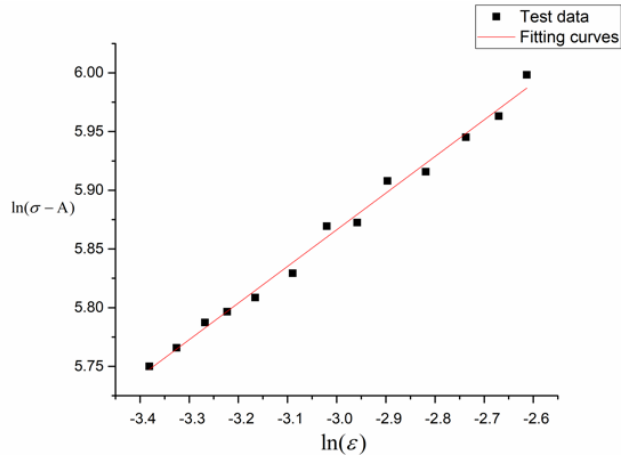

Fig. 3 Fitting curve of Aermet100 sample under quasi-static compression

The parameters C will to be determined by the parameters as mentioned above A, B and n combined with the reference temperature of Aermet100 steel (generally 298K) Hopkinson compression rod test (SHPB) data.

After removing the quasi-static reference strain rate (generally $10^{-3}s^{-1}$) condition, the Johnson cook constitutive model equation can be expressed as following:

$$\sigma = (A + B\varepsilon^{n})\left[1 + Cln(\dot{\varepsilon} / \dot{\varepsilon}_0\right]. \tag{6}$$

Under this condition, when there is no plastic strain, the above Eq. (5) becomes the following one:

$$\sigma = A\left[1 + Cln(\dot{\varepsilon} / \dot{\varepsilon}_0\right]. \tag{7}$$

Yield strength of Aermet100 at different strain rates is listed in Table 2.

Table 2

Yield strength at different strain rates

Strain rates, s^{-1}	1300	1700	2800	4300
Yield strength, MPa	2093	2105	2113	2135

According to the above formula and the data in the chart, the data processing and fitting can obtain the $\sigma - ln\ \ln(\dot{\varepsilon}/\dot{\varepsilon}_0)$ curve, as shown in Fig. 4, the fitting value R^2 of curve fitting is 0.9, and the intercept value is 1635, which is quite close to the value mentioned in the previous article. According to the above equation, the values of parameters C in the Johnson-Cook constitutive model equation of the material used in the Aermet100 steel sample test are obtained, the value is 0.019.

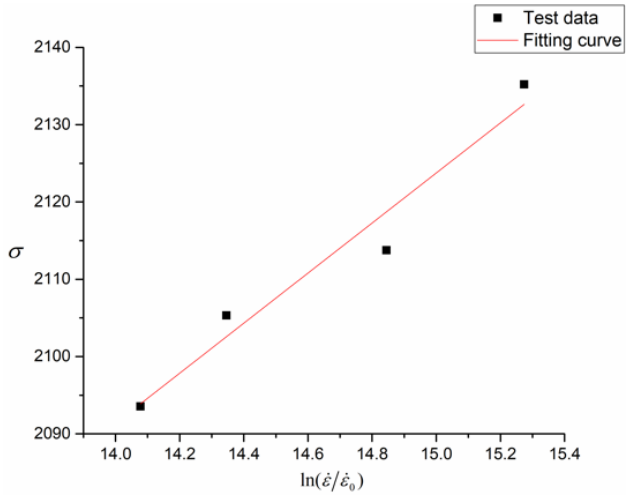

Fig. 4 Fitting curve of Aermet100 sample under SHPB test

Finally, the parameter value m is quoted from the paper "Q. sun et al., 2018" [7]. Based on the above work, the complete expression for Aermet100 steel is as following:

$$\sigma_y = (1620.59 + 879.8\varepsilon_p^{0.31232})(1 + 0.019ln\dot{\varepsilon}^{*})(1 - T^{*2.75}). \tag{8}$$

The whole model including the basic equations and the numerical integration method (See he basic equations in the Supplementary Material) is defined in the UMAT using the Fortran language, which is called in the following analysis later.

3. Extended finite element method

Belyschko and Black (1999) [8] proposed a finite element method independent of mesh generation used to solve crack propagation for the first time. Based on the traditional finite element method, the element nodes near the crack tip or the crack surface were enhanced by the near-field displacement solution of the crack to explain the appearance of cracks. The difficulty in 3D dynamic fracture

simulation is how to keep the continuity and smoothness of the crack surface and crack propagation direction. Areias and Belytschko (2005) [9] approximately satisfied the condition by adjusting the normal of the crack surface.

3.1. Introducing nodal enrichment functions

For fracture analysis, the enrichment functions typically consist of the near-tip asymptotic function which captures the singularity around the crack tip and a discontinuous function that represents the jump in displacement across the crack surface. The approximation for a displacement vector function **u** with the partition of unity enrichment is:

$$\mathbf{u} = \sum_{I=1}^{N} N_I(x)\left[\mathbf{u}_I + H(x)\mathbf{a}_I + \sum_{\alpha=1}^{4} F_\alpha(x)\mathbf{b}_I^\alpha\right], \quad (9)$$

where: $N_I(x)$ are the usual nodal shape functions. The first term on the right-hand side of the above equation, $\mathbf{u}_I$ is the usual nodal displacement vector associated with the continuous part of the finite element solution. The second term is the product of the nodal enriched degree of freedom vector $\mathbf{a}_I$ and the associated discontinuous jump function $H(x)$ across the crack surfaces. The third term consists of the product of the nodal enriched degree of freedom vector $\mathbf{b}_I^\alpha$ and the associated elastic asymptotic crack-tip functions $F_\alpha(x)$. The first term on the right-hand side is applicable to all nodes in the model; the second term is valid for nodes whose shape function support is cut by the crack interior; the third term is used only for nodes whose shape function support is cut by the crack tip.

$$H(x) = \begin{cases} 1 \text{ if } \left(\mathbf{x} - \mathbf{x}^*\right)\cdot\mathbf{n} \geq 0 \\ \text{-1 otherwise} \end{cases}, \quad (10)$$

where: **x** is a sample (Gauss) point; $\mathbf{x}^*$ is the point on the crack closest to **x** and **n** is the unit outward normal to the crack at **x**.

$$F_\alpha(x) = \\ = \left[\sqrt{r}\sin\frac{\theta}{2}, \sqrt{r}\cos\frac{\theta}{2}, \sqrt{r}\sin\theta\sin\frac{\theta}{2}, \sqrt{r}\sin\theta\cos\frac{\theta}{2}\right], \quad (11)$$

where: (r, θ) is a polar coordinate system with its origin at the crack tip and $\theta = 0$ is tangent to the crack at the tip.

3.2. Damage modelling

Damage modeling aims to simulate the degradation and eventual failure of an enriched element. The failure mechanism consists of two ingredients: a damage initiation criterion and a damage evolution law. The initial response is assumed to be linear in this study. However, once a damage initiation criterion is met, damage can occur according to a user-defined damage evolution law.

Crack initiation refers to the beginning of degradation of the cohesive response to an enriched element. The process of degradation begins when the stresses or strains satisfy specified crack initiation criteria.

An additional crack is introduced or the crack length of an existing crack is extended after an equilibrium increment when the fracture criterion f reaches the value 1.0 within a given tolerance:

$$1.0 \leq f \leq 1.0 + f_{tol}, \quad (12)$$

where: it is needed to specify the tolerance f_{tol}. If $f > 1.0 + f_{tol}$ the time increment is cut back so that the crack initiation criterion is satisfied.

1) Maximum principal strain criterion for crack initiation.

The maximum principal strain criterion can be represented as:

$$f = \left\{\frac{\langle \varepsilon_{max} \rangle}{\varepsilon^o{}_{max}}\right\}, \quad (13)$$

here: $\varepsilon^o{}_{max}$ represents the maximum allowable principal strain, and the Macaulay brackets signify that a purely compressive strain does not initiate damage. Damage is assumed to initiate when the maximum principal strain ratio (as defined in the expression above) reaches a value of one.

2) Damage evolution.

The damage evolution law describes the rate at which the cohesive stiffness is degraded once the corresponding initiation criterion is reached. A scalar damage variable D represents the averaged overall damage at the intersection between the crack surfaces and the edges of cracked elements, for example, microcracks and microvoids (Kachanov, 1986; Voyiadjis and Kattan, 2005) [10, 11]. It initially has a value of 0. If the damage evolution is modelled, D monotonically evolves from 0 to 1 upon further loading after the initiation of damage. The normal and shear stress components are affected by the damage according to:

$$t_n = \begin{cases} (1-D)T_n, T_n \geq 0 \\ T_n, \quad \text{otherwise (no damage to compressive stiffness)} \end{cases}. \quad (14)$$

$$t_n = (1-D)T_s, \quad (15)$$

$$t_t = (1-D)T_t, \quad (16)$$

where: T_n, T_s and T_t are the normal and shear stress components predicted by the elastic traction separation behavior for the current separations without damage. Loading rate fatigue tests and extended finite element model simulation.

3.3. Sample fatigue tests

The effect of loading rate on the fatigue performance of ultra-high-strength steel Aermet100 was studied. There were 500 specimens, which were divided into five groups, and there were five levels of loading time (unloading time not included) (1 s, 0.5 s, 0.3 s, 0.2 s, 0.1 s). In particular, it is worth mentioning that this fatigue test is based on force control and thus strain or displacement cannot be

obtained directly. This paper carries the following analysis and simulation with loading rate as the primary variable.

Considering the loading capacity of the testing machine, this study divided the loading rate of the sample into the following groups. Half-sine loading was used in the experiment with the maximum tensile load of 90 kN and the stress ratio is set to 0.061. Under this condition, the stress is 1650 MPa, which exceeds the yield strength of the Aermet100 steel.

Laboratory fatigue tests were carried out accordingly. From the classification of the test results of five groups of samples, the fracture position and shape can be divided into three categories: one fracture in the middle of the weak working area, one fracture in the transition section and two fractures in the working area. Specimen with two fractures was shown in Fig. 5 below.

Fig. 5 Two Fractures in the middle working area

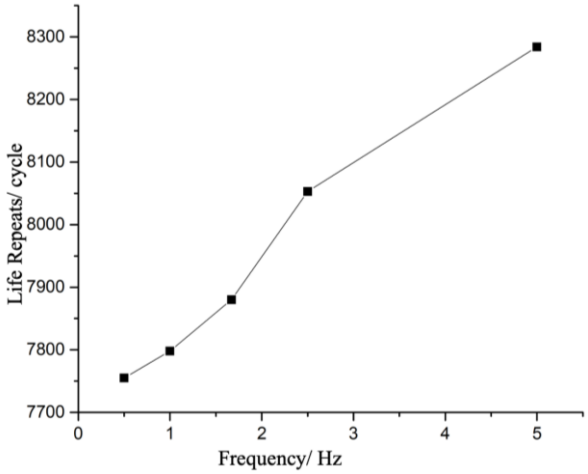

Fig. 6 Life repeats under different frequencies

After the completion of 500 Aermet100 steel specimen fatigue tests, the life repeats data were statistically divided. Fig. 6 shows the results of life cycles under different loading rates and frequencies.

3.4. Loading rate fatigue simulation

The Aermet100 specimen is modeled in ABAQUS, and the mesh is discretized. A total of 8415 nodes and 6080 meshes are generated. The element type is the hexahedral element C3D8R. The complete Aermet100 steel J-C model is written in the FORTRAN language, input by ABAQUS UMAT module, and called during the simulation.

According to the laboratory loading, the same boundary conditions and loads are applied on both sides of the specimen in the finite element model. The stress and strain plots of the sample under static load is shown in the Fig. 7.

It can be seen that under the static load, part of the weak working area of the sample has entered into the plastic, resulting in plastic deformation as shown in Figs. 8 and 9.

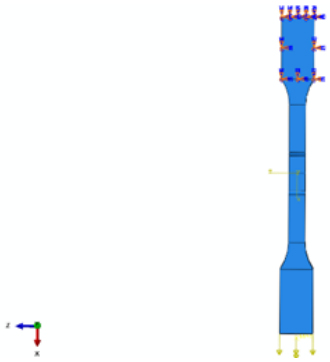

Fig. 7 Loading and boundary conditions

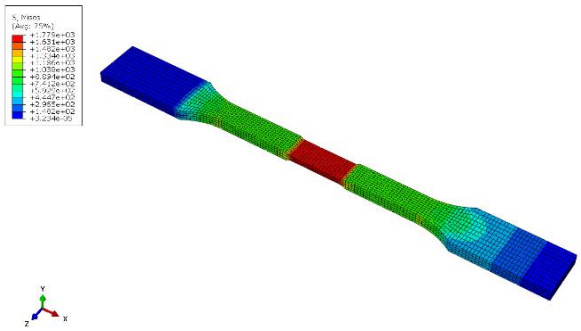

Fig. 8 Stress and plastic equivalent strain plot under statistic load

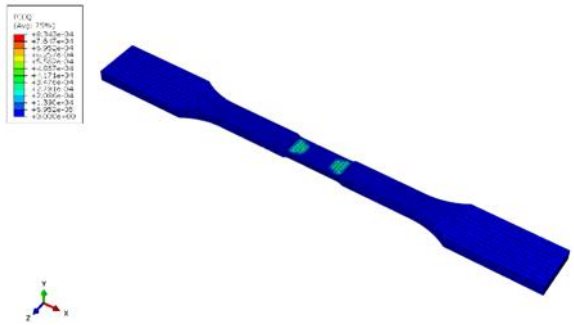

Fig. 9 Plastic equivalent strain plot under statistic load

In the following simulation, the XFEM module is introduced into the finite element simulation model, and the whole sample is set as the possible crack initiation area. The study selected the damage as MAXPE damage under transaction laws, and set the tolerance $f = 0.005$ (defined in formula 10). The low cycle fatigue life of the specimen is set at less than 20000 times, and the fatigue cycles are set to 20000 times by cyclic direct.

Due to the dispersion of the defects in the specimen, there are three different fracture positions in the specimen: the fracture in the middle section of the specimen, the fracture in the transition section of the weak zone, and two fractures in the middle section of the test. In the finite element simulation calculation model, through different fracture strain settings, three types of fractures can be observed in the same position. The range of the corresponding strain

is not discussed in detail in this paper. The average fracture strain measured at the beginning of this paper is 0.1088 in the subsequent calculation.

The following plots Figs. 10 – 12 show the simulation results.

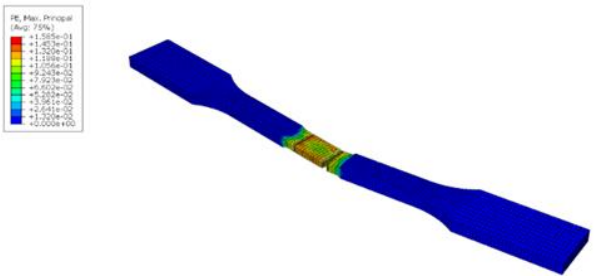

Fig. 10 Equivalent stress at fracturing time

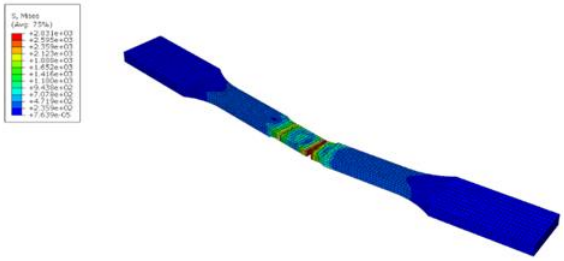

Fig. 11 Plastic strain at fracturing time

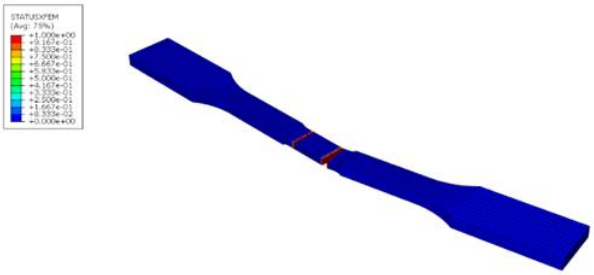

Fig. 12 Status xfem plot at fracturing time

4. Analysis of the influence of loading rate on the fatigue performance of Aermet100 steel

The simulation entirely refers to the laboratory loading conditions. It is carried out in ABAQUS according to the loading rate of five orders. The number of cycles at complete fracture is taken as the life value, as shown in Table 3 below.

Table 3

Life cycles of 5 groups

Loading rate, kN/s	Frequency, Hz	Averaged life repeats, cycle	Simulation results, cycle	Error/%
90	0.5	7755	6950	10.38
180	1	7798	7500	3.82
300	1.67	7880	7501	4.81
450	2.5	8053	7502	6.84
900	5	8284	7550	8.86

It can be seen that under the given loading rate in the laboratory, the simulation value and the test average life have a high degree of fit. The finite element dynamic simulation model based on the J-C dynamic constitutive equation and XFEM method can accurately simulate the fatigue fracture process of the Aermet100 steel sample under dynamic load.

Due to the limited loading capacity of the testing machine, when the loading rate is higher than 10 Hz, it is beyond the loading range of the testing machine. Considering the engineering application, this study set the time lower limit. Therefore, when applying the dynamic finite element simulation model, this study controls loading time range within. In this range, the specimen life repeats results are shown in Table 4.

Take the logarithm of time and draw the curve of life versus the logarithm of time as following.

Table 4

Mechanical characteristics of pipes main steel, weld and heat affected zone metal

Loading rate	Loading time, s	Simulation results, cycle
1800 kN/s	0.05	7760
4500 kN/s	0.02	8502.5
9000 kN/s	0.01	9005
18000 kN/s	0.005	9260
45000 kN/s	0.002	10505
90000 kN/s	0.001	11505
180000 kN/s	0.0005	11510
450000 kN/s	0.0002	12810
900000 kN/s	0.0001	15550

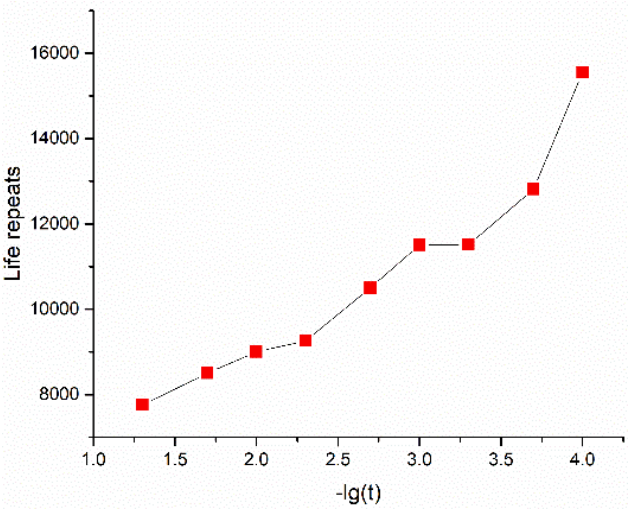

Fig. 13 Equivalent stress at fracturing time

Generally, life repeats increase with the decrease of the loading time. From Fig. 13, it can be clearly seen that when loading time is less than $10^{-1.5}$ s, the increase of life span is relatively slow, and in the time scale from $10^{-1.5}$ s to 10^{-4} s, life cycles increase rapidly.

5. Conclusions

This paper mainly focuses on the fatigue performance of ultra-high-strength steel Aermet100 under different loading rates. Due to the limitation of experimental conditions, it is hard to acquire fatigue data at high loading rates. Differently, to characterize the material properties affected by the strain rate, this paper introduces the J-C model and combined this model with the XFEM to predict the variations of the life cycles versus loading time.

1) Aermet100 steel is sensitive to the strain rate. Based on the test data, the Johnson-Cook constitutive model fitted by the least square method takes the strain rate into account, which solves the strain hardening problem caused

by the strain rate change of high strength steel resulted from the loading rate.

2) Based on the ductile fracture mechanics of the plastic damage model, the XFEM method combined with the J-C constitutive equation considering the strain rate effect was used to simulate the fatigue behavior of Aermet100 steel under dynamic load.

3) In the loading time range of 0.0001 ~ 1s, the fatigue test of load rate on fatigue life of Aermet100 high strength steel shows that when the loading rate is low, the influence on the fatigue life is small; through simulation, the variation law of sample life with loading rate can be obtained. With the increase in the loading rate, the life cycles of the sample increase. To be specific, life cycles significantly increase when the loading time is 10^{-4} s.

References

1. **Zejian, X. U.; Yulong, L. I.** 2006. Effect of loading rate on mode in dynamic fracture toughness of high strength steels 40Cr AND 30CrMnSiNi2A, Acta Metallurgica Sinica 42(009): 965-970. http://dx.doi.org/10.1016/j.actamat.2006.05.031.
2. **Zejian, X. U.; Yulong, L. I.; Yuanyong, L.** 2006. Mode ii dynamic fracture toughness of two high strength steels under high loading rate, Acta Metallurgica Sinica 42(6): 635-640. http://dx.doi.org/10.3321/j.issn:0412-1961.2006.06.013.
3. **Campbell, J. D.; Cooper, R. H.** 1966. Yield and flow of low-carbon steel at medium strain rates, Proceedings of the Conference on the Physical Basis of Yield and Fracture, Institute of Physics and Physical Society, London, p. 77-87.
4. **Manjoine, M. J.** 1944. Influence of rate of strain and temperature on yield stresses of mild steel, Journal of Applied Mechanics 11:211-218. http://dx.doi.org/10.1115/1.4009394.
5. **He, J.; Chen, J.; Sun, Q**. 2014. Effect of loading rate on low-cycle fatigue properties of turbine rotor steel, Procedia Materials Science 3(2):1773-1779. http://dx.doi.org/10.1016/j.mspro.2014.06.286.
6. **Johnson, G. R.; Cook, W. H.** 1983. A constitutive model and data for metals subjected to large strains, high strain rates and high temperatures, Proceedings of the 7th International Symposium on Ballistics 21: 541-547.
7. **Sun, Q. ; Liu, X. R. ; Liang, K.** 2018. Impact fatigue life prediction for notched specimen of steel AerMet100 subjected to high strain rate loading, International Journal of Applied Mechanics. http://dx.doi.org/10.1142/S1758825118500308.
8. **Belytschko, T.; Black, T**. 1999. Elastic crack growth in finite elements with minimal remeshing, International Journal for Numerical Methods in Engineering. http://dx.doi.org/10.1002/(SICI)10970207(19990620)45:5<60:AID-NME598>3.0.CO;2-S.
9. **Pedro, M, A**. 2005. Non-linear analysis of shells with arbitrary evolving cracks using XFEM, International Journal for Numerical Methods in Engineering. http://dx.doi.org/10.1002/nme.1192.
10. **Kachanov, L. M.; Krajcinovic, D**. 1986. Introduction to continuum damage mechanics, Journal of Applied Mechanics 54(2): 481.
11. **Voyiadjis ,G. Z.; Al-Rub, R. K. A**. 2005. Gradient plasticity theory with a variable length scale parameter, International Journal of Solids & Structures 42(14): 3998-4029. http://dx.doi.org/10.1016/j.ijsolstr.2004.12.010.

E. Zhu, H. Chen, X. Fang, X. Wei, H. Nie

EXPERIMENTAL RESEARCH AND FATIGUE LIFE PREDICTION OF ULTRA-HIGH-STRENGTH STEEL AERMET100

S u m m a r y

This study concentrates on the fatigue performance of ultra-high-strength steel Aermet100 under different loading rates. The standard specimen measured the static mechanical properties of Aermet100 steel, based on which the basic mechanical properties and fracture characteristics of the sample before and after necking was obtained. To take the strain rate effect into account, this study uses the dynamic constitutive model Johnson-Cook. The equation parameters are fitted through dynamic mechanical tests and quasi-static tests. This model is input into ABAQUS user-defined program afterward. Referring to the work done above, along with the extended finite element method (XFEM), this study establishes the dynamic fracture finite element model of the Aermet100 steel specimen on the basis of the continuous damage mechanics. Five groups of specimen fatigue tests were carried out in the laboratory. Simulation results show the feasibility and accuracy of the integrated XFEM model with the same loading and boundary conditions. The experimental data and simulation results prove that, in the loading time range of 0.0001 ~ 1s, the life cycles increase as the loading rate increases. It is worth mentioning that when the loading time is in the order of 0.0001s, the life changes significantly.

Keywords: ultra-high-strength steel Aermet100; fatigue performance; Johnson-Cook; loading rate; XFEM.

Received June 18, 2021
Accepted April 08, 2022